

Extracting information from the data flood of new solar telescopes. Brainstorming

A. Asensio Ramos^{1,2}

¹*Instituto de Astrofísica de Canarias, 38205, La Laguna, Tenerife, Spain*

²*Departamento de Astrofísica, Universidad de La Laguna, E-38205 La Laguna, Tenerife, Spain*

Abstract. Extracting magnetic and thermodynamic information from spectropolarimetric observations is a difficult and time consuming task. The amount of science-ready data that will be generated by the new family of large solar telescopes is so large that we will be forced to modify the present approach to inference. In this contribution, I propose several possible ways that might be useful for extracting the thermodynamic and magnetic properties of solar plasmas from such observations quickly.

1. Introduction

In the last decades, night-time telescopes have systematically increased the diameter of the primary mirror. Today, several facilities of the 10m class (VLT, Keck, GTC, ...) are producing top quality science and projects for 20-40m class telescopes are already very advanced. On the contrary, the diameter of solar telescopes has not increased much in the last decades. Today, the most successful telescopes have primary mirrors in the range from 40 cm to 1 m and they exist since the 90s. The new generation of solar telescopes has increased the size of the primary mirror to the 1.5m class (NST, GREGOR). This slow increase in the diameter is partly motivated by the technical difficulty of heat rejection that is posed when a very large primary mirror is used. However, the ATST (in the very early phases of construction) and EST (in design phase) telescopes, belonging to the 4m class, will open a completely new window to the investigation of the Sun.

Such large photon collectors, when combined with advanced instrumentation, will allow us to obtain observations of the solar atmosphere with extraordinary spatial resolution, temporal cadence and polarimetric sensitivity. Two-dimensional spectropolarimetry on 2k×2k cameras on dozens of wavelengths with a time cadence of several seconds during observing periods of hours (thanks to the presence of multi-conjugate adaptive optics systems) will be custom. Such amount of data (especially when several instruments work simultaneously, which is one of the requisites of the new 4m class telescopes) will challenge the designers of the storage infrastructure. Even more complicated is the challenge posed to the researchers in charge of extracting physical information from the observations. Although not all observations will be analyzed with inversion codes, the inversion community has to have in mind the enormous amount of data produced by such instruments and face the challenge of developing inversion tools that can extract thermodynamic and magnetic properties at such rate. Just as an example, an instrument with a 2000×2000 camera observing one or several spectral lines

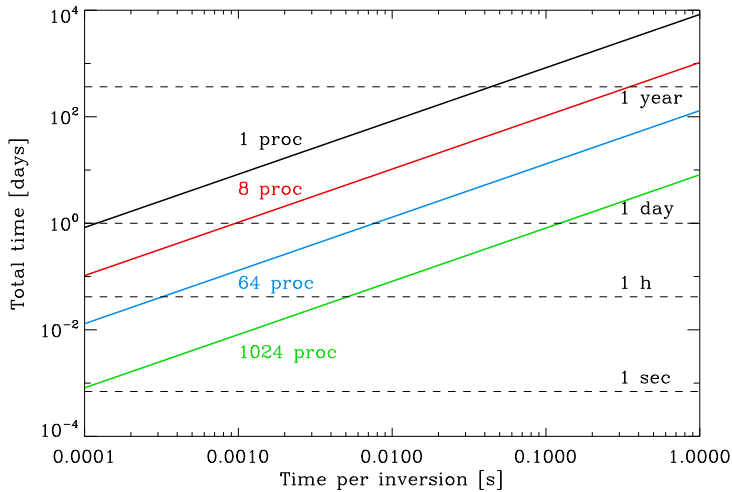


Figure 1. Total computing time for the inversion of 720 million profiles depending on the time for one single inversion. The solid color lines indicate the computing time for computer clusters of different sizes.

during three hours at a cadence of one observation per minute will produce 720 million line profiles for later analysis. If we consider an inversion method that can invert one profile per second, one would need 22.8 years to invert the full dataset (and that is only 3 hours of observations). This figure goes down to 8.3 days if an inversion is done every millisecond (or if 1000 processors are working on the problem with 1 s inversions).

A summary of the previous computations is shown in Figure 1. The color lines in the figure represent the total amount of time (in days) needed for inverting 720 million profiles depending on the computing time per inversion (in seconds). One can see that, if only one processor is used, the total computation time goes down to one day if the computation time per inversion is as low as 0.1 ms. If one wants to carry out a systematic inversion of all observations (assuming an average of 3 hours of good observing time per day) on a day-to-day basis, inversions need to be carried out in less than 0.1 ms. Equivalently, if a dedicated cluster of 1000 processors is used for this purpose, the time per inversion can be safely increased to 0.1 s without too much impact.

Such reduced computing times per inversion can be reached with fast computers for simple Milne-Eddington atmospheres using optimized codes like VFISV (Borrero et al. 2007, 2010) tailored to the inversion of a very specific dataset. This code is presently used for the inversion of filterpolarimetric data of the Helioseismic and Magnetic Imager (HMI; onboard the Solar Dynamics Observatory). One can expect that the computing power increases following Moore's law and that computers at the time when ATST and EST start observing can be a factor 8-32 faster (computers duplicate the number of transistors every 2-3 years) than present day computers. Another possibility is to consider the application of graphical processing units (GPU) to the inversion problem. The advantages of GPUs rely on the reduced price and the enormous parallelization capabilities for data-parallel computations. It remains to be investigated to what extent GPUs can accelerate the inversion process. An additional option is to use hardware

solutions like FPGAs (field programmable gate arrays) that can be configured for the inversion process (of relatively simple models because of the complexity of programming such devices). This option is considered for the onboard inversion of data for the Polarimetric and Helioseismic Imager (PHI) onboard Solar Orbiter.

The main difficulty with all these approaches lies in the fact that the inversion of chromospheric lines (which are in the mandatory list of spectral lines for both ATST and EST) is not as simple as the inversion of photospheric lines. Inversion of photospheric lines can be easily done in local thermodynamical equilibrium (LTE), which speeds up the computations. On the contrary, chromospheric lines tend to have large non-LTE corrections and the full radiative transfer problem has to be solved in each step of the iterative inversion process. This drastically increases the computation time and it is very complicated to do inversions in less than a few seconds. This is the case of NICOLE (Socas-Navarro, de la Cruz Rodríguez, Asensio Ramos, Trujillo Bueno & Ruiz Cobo, in preparation), to my knowledge, the only inversion code that solves the full non-LTE problem (neglecting the presence of atomic polarization). Additionally, these lines are formed in regions where scattering effects are important and, consequently, the polarization signals have strong contributions (or are even dominated) by atomic polarization induced by anisotropic pumping. The inversion of Stokes profiles dominated by atomic polarization is even more computationally intensive and the only existing codes that can cope with such a problem are Hazel (Asensio Ramos et al. 2008) and Helix+ (an updated version of the code used by Lagg et al. 2004, 2007), both based on a Levenberg-Marquardt (LM) algorithm, and the code of (López Ariste & Casini 2005) based on a look-up table. Hazel has been recently parallelized to cope with large-scale inversions, scaling roughly linearly with the number of processors.

The previous considerations force us to consider how to approach the inversion of photospheric and chromospheric lines with large telescopes. I will consider in this contribution several options that we would need to investigate in depth (and other options that can be derived from them) and that can help us face the problem with success.

2. Classification

The conclusion from the previous paragraphs is that the number of profiles that we need to invert is extraordinarily large. We have to change the paradigm and admit that we cannot look at all data (we lack the manpower for that even if the computing power is available). A possible option to overcome the difficulties is to apply algorithms that reduce the number of profiles to something we can deal with. We can develop automatic algorithms that can classify the observed profiles as intrinsically interesting or uninteresting. These algorithms have to work online in the telescope and either raise flags to classify them for later consideration or just throw away all uninteresting information (which is probably not welcomed by the solar community, although it is the standard procedure in other fields like in experimental particle physics). These online algorithms should ideally be based on supervised classification that need to be trained in advance. Therefore, we first have to solve the problem of defining what is interesting and what is not. Technically, we can choose among artificial neural networks (ANN), support vector machines (SVM) or Gaussian processes (GP). All of them have demonstrated robust classification capabilities once trained appropriately.

A less aggressive option is to consider unsupervised classification and dimensionality reduction methods once all the data has been stored. A line profile sampled at n

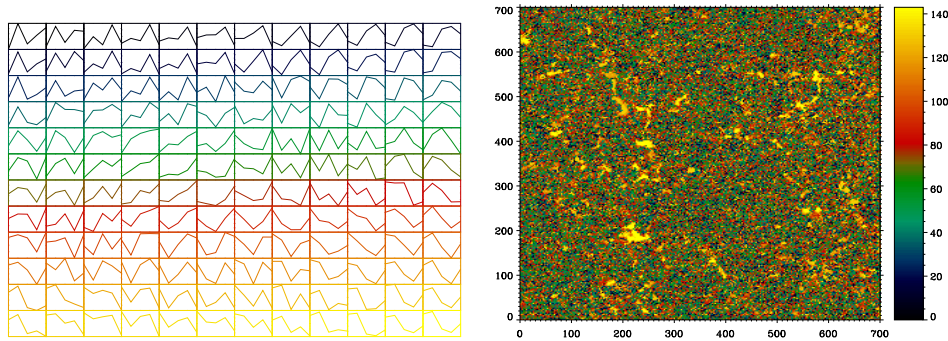


Figure 2. The left panel shows a 12×12 self-organizing map applied to the Stokes V profile of a snapshot of 5-point IMaX data. The SOM has classified similar profiles in nearby regions. By transforming the five-dimensional space of IMaX profiles to a two-dimensional space, we can easily identify anomalous profiles. The right panel displays in colors the class (from the 144 possible classes) to which every profile in the map belongs.

wavelength points can be represented as a point in the n -dimensional space \mathbb{R}^n . Although this space can have very large dimensionality, physics and the measuring instrument incorporates correlation among the different wavelength points. Consequently, the effective dimensionality of the measured Stokes profiles is decreased because they “live” in a low-dimensionality manifold of the n -dimensional space. Therefore, dimensionality reduction methods try to capture this behavior and present the user with a simplified version of the observations. The self-organizing map (SOM) belongs to this category of dimensionality reduction methods. It is an ANN where each neuron is characterized by an n -dimensional vector that represents a Stokes profile. It is trained using unsupervised learning techniques to produce a low-dimensional representation of the training sample. This representation tries to preserve the topological properties of the input space (training samples), so that nearby samples are mapped into nearby neurons (Kohonen 2001). One of its most important applications is for visualization of high-dimensional data. This method has been used by Asensio Ramos et al. (2007a) to classify profiles of the Mn I line at 15262.702 \AA . I refer to that paper for more details. After convergence of the map, the profile associated to each neuron tends to be associated with *patterns* in the input data, with similar patterns being located in nearby neurons. Consequently, once trained with some data, it is possible to use the map to classify any additional input vector, whether it was in the training set or not. The euclidean distance is calculated between the input vector and all the profiles associated to the neuron. The neuron closest to the input vector will give the class. An example of this procedure is shown in Fig. 2, where we have trained a SOM with Stokes V profiles obtained from IMaX observations (Martínez Pillet et al. 2011) onboard the Sunrise balloon (Solanki et al. 2010). The left panel displays the classes in a 12×12 array, while the right panel shows the class to which each pixel is associated. Anomalous profiles can be identified in the SOM and their physical locations easily discovered.

3. Look-up databases

In addition to the computational problem all inversion codes based on the LM algorithm suffer from, they also have problems defining realistic error bars, specially when ambiguities are present. Realistic error bars can be obtained using a fully Bayesian approach (Asensio Ramos et al. 2007b), with the inconvenience of increasing the computational problem because a Montecarlo approach (thus requiring many evaluations of the forward problem) is used to sample the posterior distribution.

One approach that has been demonstrated to partially solve both problems is the one of building large databases. The database contains many Stokes profiles evaluated at all physically relevant combination of the parameters of the model under consideration. A direct comparison of the observed profile with all the profiles present in the database gives us an estimation of the model parameters. Additionally, error bars (although not fully Bayesian) can be estimated taking into account all profiles inside a ball around the best model. The database approach works well although the inherent flexibility of LM codes has to be sacrificed because the database has to be built in advance. The database approach has been pursued by López Ariste & Casini (2002), Casini et al. (2005), López Ariste & Casini (2005) and Casini et al. (2009) with great success. Its application to the very complex problem of scattering polarization and the Hanle effect is specially relevant because the database needs to be computed only once and then can be applied without much computational burden to the observations.

Building the database is not an easy task because it might suffer from the curse of dimensionality. This is related to the fact that, when the dimensionality of a space increases, the volume of the space increases so fast that any available sampling becomes sparse. In other words, the size of a database should increase exponentially fast with the number of wavelength points of the sampled Stokes profiles. Fortunately, this is partially solved because the assumed parametric models that generate the Stokes profiles efficiently reduce the dimensionality of the problem (inducing that the Stokes profiles lay in a low-dimension manifold of the full space). Casini, López Ariste and co-workers have developed Montecarlo algorithms to efficiently build the database. Additionally, instead of storing the full Stokes parameters in the database, they project them to a small subset of principal components, gaining compression and reducing the dimensionality of the problem.

When the mapping between the input model parameters and the output Stokes parameters is complex (like when scattering polarization and the Hanle effect play a role) and the noise level of the observations is small, the size of databases has to be increased dramatically. Above a certain size of the database, the search algorithm turns out to be slower than an inversion code based on the LM algorithm like Hazel. For a database with n Stokes profiles, the search scales as $O(n)$. There is not much room for improving the search because only a few methods seem to be significantly better than a brute-force computation of all distances. However, by relaxing the problem and computing nearest neighbors approximately, it is possible to achieve significantly faster running times (of the order of 1-2 orders of magnitude) often with a relatively small actual errors.

An option for very large databases is to reduce its size using a SOM and use it for inversion purposes to give a rough estimation of the model parameters. To show this, I have trained a 30×30 SOM using the Stokes I profiles for the 10830 Å multiplet kindly provided by R. Casini from the database used by Casini et al. (2009). We extract the temperature, optical depth and velocity of each one of the profiles associated to a given

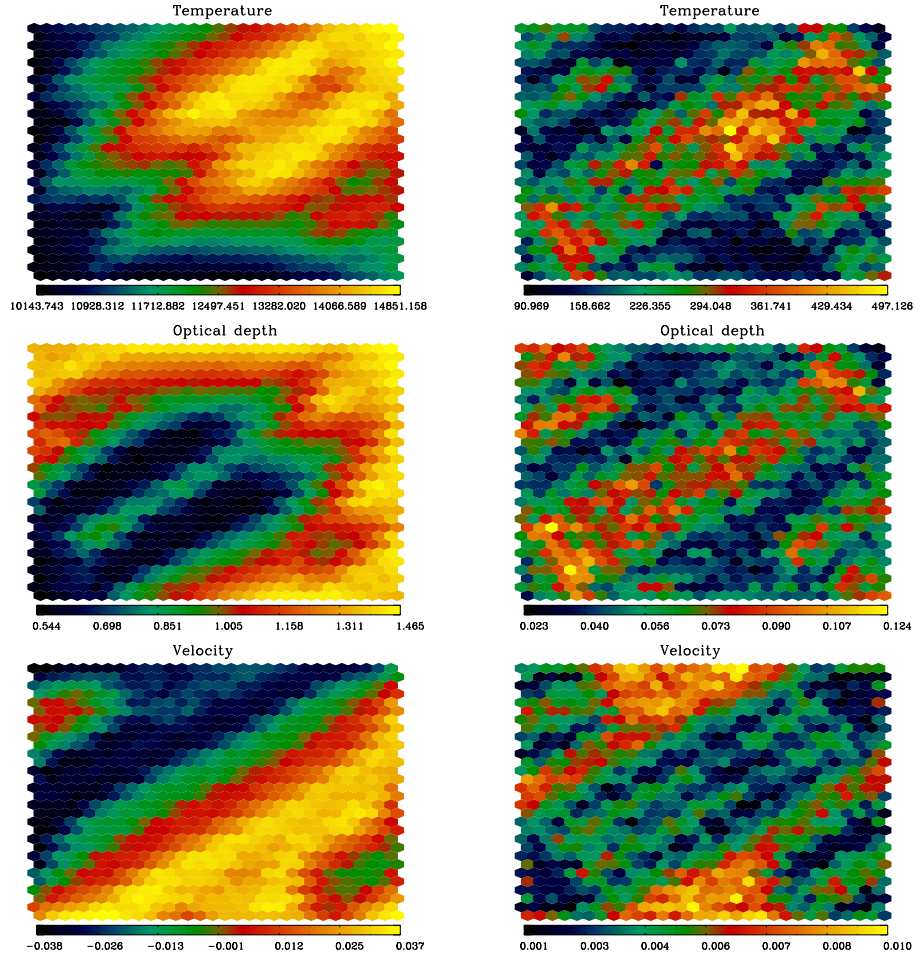


Figure 3. The left columns show the temperature (upper panel, in K), optical depth (middle panel) and velocity (lower panel, in km s^{-1}) associated to each neuron of the SOM trained on a set of Stokes I profiles of the 10830 Å multiplet. It is computed as the mean of all profiles in the training database that are associated with each neuron. The right panels display the associated standard deviation. This SOM can be used to quickly estimate the physical parameters from the observables.

neuron, compute its average and the standard deviation. The results are shown in Fig. 3. This demonstrates that, presenting a new observation to the SOM and picking up the neuron giving the smallest euclidean distance, gives an estimation of the temperature, optical depth and velocity with a small error associated. One of the advantages of this fast inversion is that one only needs to compare the input Stokes profiles with 900 profiles, instead of the full database. If only approximate values of the physical parameters are desired, this might give a large improvement in terms of computation work.

4. Emulators

We have stated that standard inversion tools are quite slow when the forward problem is complex. A possible solution to this issue lies on the application of emulators. We call an emulator any machine learning method that “learns” the mapping between the thermodynamic and magnetic parameters (expressed in vector form as θ) and the emergent Stokes profiles, $[I(\lambda), Q(\lambda), U(\lambda), V(\lambda)]$. The main advantage of this approach is that, if the selected machine learning method, once trained, is faster than solving the full problem, we can apply a standard LM algorithm to carry out the inversion. Additionally, increasing the speed of the computation of the forward model opens up the option of carrying out Bayesian inversion through the use of efficient Markov Chain Monte Carlo methods. ANNs, GPs and SVMs are standard machine learning methods that can be used to learn the mapping. In order to simplify the problem, the Stokes profiles can be decomposed as a linear combination of the principal components, so that the mapping to be learnt is between θ and the projection of every Stokes profile along the principal components.

The main difficulty of this approach resides on the precision that needs to be imposed to the mapping. If the noise in the observation is characterized by a standard deviation σ , the machine learning method needs to synthesize profiles that are, for a set of thermodynamic and magnetic parameters, closer than σ to the correct synthetic profiles in order not to introduce artificial biases. This is a very complicated task and more work needs to be done. As an example, Asensio Ramos & Ramos Almeida (2009) uses an ANN to synthesize spectral energy distributions of the clumpy dusty tori models of Nenkova et al. (2008). The restrictions put to these ANNs are very relaxed given the large observational errors. The synthesis of Stokes profiles is much more restrictive in terms of precision.

One possible improvement in the quality of emulators resides in modifying the decomposition of the Stokes profiles. The projection along the principal components is a linear transformation in the space of Stokes profiles. It can be understood as a rotation in an euclidean space and a projection along a low-dimensional hyperplane. As a consequence, it is not able to capture the shape of the manifold where the Stokes profiles live. This poses more difficulties to the machine learning method that needs to capture the non-linear behavior of the manifold. Fortunately, more elaborate non-linear dimensionality reduction techniques like diffusion maps (Coifman & Lafon 2006; Lafon & Lee 2006), locally linear embedding (Roweis & Saul 2000), isomap (Tenenbaum et al. 2000), kernel-PCA (Schölkopf et al. 1998) and autoassociative artificial neural networks (Socas-Navarro 2005) exist. In principle, one could think that allowing the dimensionality reduction to capture part of the non-linearity of the manifold will help any machine learning method to learn the mapping between the input parameters and the Stokes profiles. This possibility needs to be investigated in more detail. The same strategy could also be applied for improving machine learning methods that learn directly the mapping between the Stokes profiles and the physical parameters.

5. Model selection

As stated above, inferring magnetic and thermodynamic information from spectropolarimetric observations relies on the assumption of a parameterized model atmosphere whose parameters are tuned by comparison with observations. Often, the choice of the

underlying atmospheric model is based on subjective reasons. In other cases, complex models are chosen based on objective reasons (for instance, the necessity to explain asymmetries in the Stokes profiles) but it is not clear what degree of complexity is needed. The lack of an objective way of comparing models has, sometimes, led to opposing views of the solar magnetism because the inferred physical scenarios are essentially different. This can be solved using Bayesian model selection tools, allowing us to determine which is the model best suited for explaining the Stokes profiles observed in a pixel (e.g., Trotta 2008, for a general description and more details). Let's assume we have N_{mod} models $\{\mathcal{M}_i, i = 1 \dots N_{\text{mod}}\}$ competing to explain the same set of observations formally represented by D . Here, D will be represented by a formal vector $\mathbf{d} = [I(\lambda_1), I(\lambda_2), \dots, Q(\lambda_1), \dots, U(\lambda_1), \dots, V(\lambda_1), \dots]$ whose elements are the values of the Stokes parameters I , Q , U , and/or V at certain wavelengths $\lambda_1, \lambda_2, \dots$. By a *model* we mean an algorithm that depends on a set of $N_j^{(i)}$ parameters $\boldsymbol{\theta}_i = (\theta_{i,1}, \theta_{i,2}, \dots, \theta_{i,N_j^{(i)}})$ (often, the temperature at one or several points in a model atmosphere; the magnetic field strength, in clination, and azimuth; the density, etc), whose output is a prediction $\mathbf{y}(\boldsymbol{\theta}_i)$ of the data. The Bayes theorem (Jaynes 2003; MacKay 2003; Gregory 2005) states that the posterior probability of each model at the light of the observed data is

$$p(\mathcal{M}_i|D) = \frac{p(D|\mathcal{M}_i)p(\mathcal{M}_i)}{p(D)}, \quad (1)$$

where $p(\mathcal{M}_i)$ is our prior belief in each model (which we will assume to be the same for all the models considered here; see below), while $p(D)$ is just a normalization constant:

$$p(D) = \sum_{i=1}^{N_{\text{mod}}} p(D|\mathcal{M}_i)p(\mathcal{M}_i). \quad (2)$$

Finally, $p(D|\mathcal{M}_i)$ is the evidence or marginal likelihood, which is the key ingredient of our model comparison, and is given by the following integral (e.g., Trotta 2008; Asensio Ramos 2011):

$$p(D|\mathcal{M}_i) = \int d\boldsymbol{\theta}_i p(\boldsymbol{\theta}_i|\mathcal{M}_i)p(D|\boldsymbol{\theta}_i, \mathcal{M}_i). \quad (3)$$

The quantity $p(\boldsymbol{\theta}_i|\mathcal{M}_i)$ is the prior distribution for the model parameters. The quantity $p(D|\boldsymbol{\theta}_i, \mathcal{M}_i)$ in Eq. (3) is the likelihood, which is computed from the observed data. Assuming that the observations are corrupted with uncorrelated Gaussian random noise, then

$$p(D|\boldsymbol{\theta}_i, \mathcal{M}_i) = \prod_{j=1}^M (2\pi\sigma_j^2)^{-1/2} \exp\left[-\frac{(y_j(\boldsymbol{\theta}_i) - d_j)^2}{2\sigma_j^2}\right], \quad (4)$$

(for more details, see Asensio Ramos et al. 2007b; Asensio Ramos 2009). It is important to note that, if a model parameter is completely unconstrained by the observed data (so the ensuing likelihood does not depend on this parameter), the evidence does not penalize it because it factorizes from the integral.

Given two models, \mathcal{M}_0 and \mathcal{M}_1 that are proposed to explain an observation, the ratio of posteriors

$$\frac{p(\mathcal{M}_0|D)}{p(\mathcal{M}_1|D)} = \frac{p(\mathcal{M}_0)}{p(\mathcal{M}_1)} \frac{p(D|\mathcal{M}_0)}{p(D|\mathcal{M}_1)}, \quad (5)$$

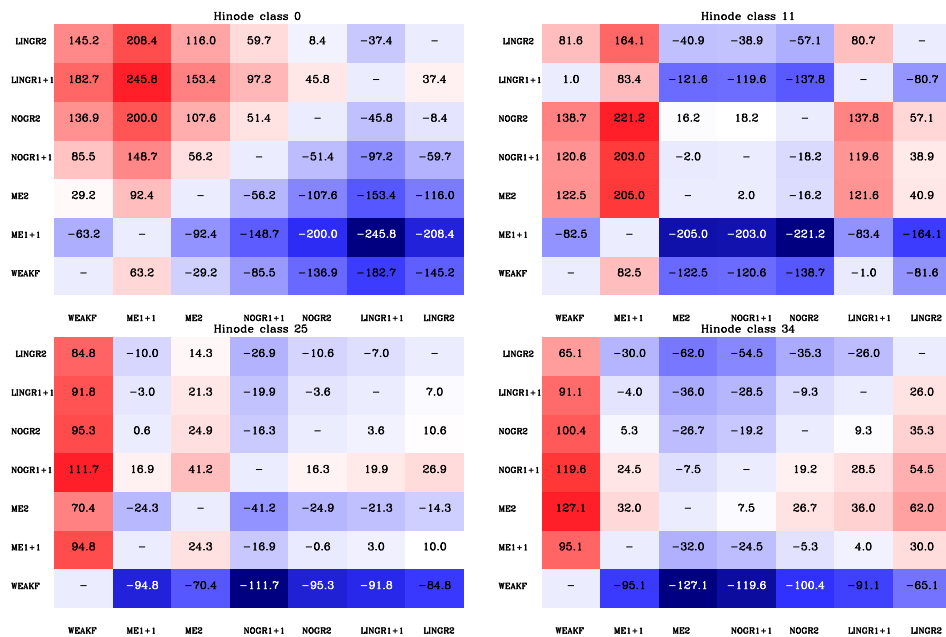


Figure 4. Logarithmic evidence ratio from each model with respect to the every other model. We show the results for four different profiles belonging to different classes as defined by Viticchié et al. (2011). Models can be compared using these tables if we assume the same a-priori probability for all of them. Each square reports the log evidence ratio between a given model in the vertical axis versus a certain model in the horizontal axis. Red and yellow colors indicate when the model in the vertical axis is more probable and blue when the opposite happens. Note that these tables are symmetric with respect to the diagonal.

is used to compute how more probable one model is with respect to the other (Jeffreys 1961). The ratio of evidences is known as the Bayes factor, B_{01} , and it is trivially given by:

$$B_{01} = \frac{p(D|M_0)}{p(D|M_1)}. \quad (6)$$

If both models are assumed to have the same a-priori probability (which is what we have assumed in all subsequent computations), the ratio of posteriors is just the Bayes factor. Large values of B_{01} indicate a preference for model M_0 while small values indicate a preference for model M_1 . The modified Jeffreys scale can be used to translate values of the Bayes factor into strengths of belief (Jeffreys 1961; Kass & Raftery 1995; Gordon & Trotta 2007).

It is illustrative to consider model selection in a league framework (model vs. model for explaining a certain observation). This is shown in Fig. 4, where each square indicates the value of the logarithmic evidence ratio obtained from the competition of pairs of models. Red colors are associated to a model on the horizontal axis that is preferable to a model in the vertical axis. Obviously, only half of the squares contain relevant information.

Given that calculating a reliable estimation of the evidence is computationally very demanding, it is of interest to compare it with simpler proxies used for model

comparison. The property of such proxies is that they can be calculated very fast and it is not necessary to perform the multidimensional integral of the evidence. The Bayesian Information Criterion (BIC; Schwarz 1978) is one of the routinely used proxies. It is based on the crude approximation of gaussianity of the posterior with respect to the model parameters but it is extremely simple to calculate:

$$\text{BIC} = \chi_{\min}^2 + k \ln N \quad (7)$$

(8)

where k is the number of free parameters of the model, N is the number of observed wavelength points and χ_{\min}^2 is:

$$\chi_{\min}^2 = \sum_{j=1}^M \left(\frac{y_j(\widehat{\boldsymbol{\theta}}) - d_j}{\sigma_j} \right)^2, \quad (9)$$

the minimum value of the χ^2 merit function attained for the vector of model parameters $\widehat{\boldsymbol{\theta}}$. In the previous formula, d_j is each one of the M observed wavelength points (including the four Stokes parameters), σ_j is the standard deviation of the noise and $y_j(\widehat{\boldsymbol{\theta}})$ is the Stokes profiles predicted for the vector of model parameters $\widehat{\boldsymbol{\theta}}$.

When comparing several models, the model with the smallest value of the BIC is the preferred one. We have verified that more than 80% of the time the BIC picks up the same model selected by the evidence ratio. Consequently, we suggest anyone carrying out inversions to compute the value of the BIC for the selected model. This will facilitate model comparison in the future.

Acknowledgments. Financial support by the Spanish Ministry of Science and Innovation through projects AYA2010-18029 (Solar Magnetism and Astrophysical Spectropolarimetry) and Consolider-Ingenio 2010 CSD2009-00038 is gratefully acknowledged.

References

- Asensio Ramos, A. 2009, *ApJ*, 701, 1032
 — 2011, in *Astronomical Society of the Pacific Conference Series*, edited by J. R. Kuhn, D. M. Harrington, H. Lin, S. V. Berdyugina, J. Trujillo-Bueno, S. L. Keil, & T. Rimmele, vol. 437 of *Astronomical Society of the Pacific Conference Series*, 135
 Asensio Ramos, A., Martínez González, M. J., López Ariste, A., Trujillo Bueno, J., & Collados, M. 2007a, *ApJ*, 659, 829
 Asensio Ramos, A., Martínez González, M. J., & Rubiño Martín, J. A. 2007b, *A&A*, 476, 959
 Asensio Ramos, A., & Ramos Almeida, C. 2009, *ApJ*, 696, 2075. 0903.0622
 Asensio Ramos, A., Trujillo Bueno, J., & Landi Degl'Innocenti, E. 2008, *ApJ*, 683, 542
 Borrero, J. M., Tomczyk, S., Kubo, M., Socas-Navarro, H., Schou, J., Couvidat, S., & Bogart, R. 2010, *Sol. Phys.*, 35
 Borrero, J. M., Tomczyk, S., Norton, A., Darnell, T., Schou, J., Scherrer, P., Bush, R., & Liu, Y. 2007, *Sol. Phys.*, 240, 177
 Casini, R., Bevilacqua, R., & López Ariste, A. 2005, *ApJ*, 622, 1265
 Casini, R., López Ariste, A., Paletou, F., & Léger, L. 2009, *ApJ*, 703, 114. 0906.2144
 Coifman, R. R., & Lafon, S. 2006, *Appl. Comput. Harmon. Anal.*, 21, 5
 Gordon, C., & Trotta, R. 2007, *MNRAS*, 382, 1859. 0706.3014

- Gregory, P. C. 2005, *Bayesian Logical Data Analysis for the Physical Sciences* (Cambridge: Cambridge University Press)
- Jaynes, E. T. 2003, *Probability Theory: The Logic of Science* (Cambridge: Cambridge University Press)
- Jeffreys, H. 1961, *Theory of Probability* (Oxford: Oxford University Press)
- Kass, R., & Raftery, A. 1995, *J. Am. Stat. Assoc.*, 90, 773
- Kohonen, T. 2001, *Self-organizing maps* (Berlin: Springer)
- Lafon, S., & Lee, A. 2006, *IEEE Trans. Pattern Anal. Mach. Intell.*, 28, 1393
- Lagg, A., Woch, J., Krupp, N., & Solanki, S. K. 2004, *A&A*, 414, 1109
- Lagg, A., Woch, J., Solanki, S. K., & Krupp, N. 2007, *A&A*, 462, 1147
- López Ariste, A., & Casini, R. 2002, *ApJ*, 575, 529
- 2005, *A&A*, 436, 325
- MacKay, D. J. C. 2003, *Information Theory, Inference, and Learning Algorithms* (Cambridge University Press)
- Martínez Pillet, V., Del Toro Iniesta, J. C., Álvarez-Herrero, A., Domingo, V., Bonet, J. A., González Fernández, L., López Jiménez, A., Pastor, C., Gasent Blesa, J. L., Mellado, P., Piqueras, J., Aparicio, B., Balaguer, M., Ballesteros, E., Belenguer, T., Bellot Rubio, L. R., Berkefeld, T., Collados, M., Deutsch, W., Feller, A., Girela, F., Grauf, B., Heredero, R. L., Herranz, M., Jerónimo, J. M., Laguna, H., Meller, R., Menéndez, M., Morales, R., Orozco Suárez, D., Ramos, G., Reina, M., Ramos, J. L., Rodríguez, P., Sánchez, A., Uribe-Patarroyo, N., Barthol, P., Gandorfer, A., Knoelker, M., Schmidt, W., Solanki, S. K., & Vargas Domínguez, S. 2011, *Sol. Phys.*, 268, 57
- Nenkova, M., Sirocky, M. M., Ivezić, v., & Elitzur, M. 2008, *ApJ*, 685, 147
- Roweis, S., & Saul, L. K. 2000, *Science*, 290, 2323
- Schölkopf, B., Smola, A. J., & Müller, K.-R. 1998, *Neural Computation*, 10, 1299
- Schwarz, G. E. 1978, *The Annals of Statistics*, 6, 461
- Socas-Navarro, H. 2005, *ApJ*, 620, 517
- Solanki, S. K., Barthol, P., Danilovic, S., Feller, A., Gandorfer, A., Hirzberger, J., Riethmüller, T. L., Schüssler, M., Bonet, J. A., Martínez Pillet, V., del Toro Iniesta, J. C., Domingo, V., Palacios, J., Knölker, M., Bello González, N., Berkefeld, T., Franz, M., Schmidt, W., & Title, A. M. 2010, *ApJL*, 723, L127
- Tenenbaum, J. B., de Silva, V., & Langford, J. C. 2000, *Science*, 290, 2319
- Trotta, R. 2008, *Contemporary Physics*, 49, 71
- Viticchié, B., Sánchez Almeida, J., Del Moro, D., & Berrilli, F. 2011, *A&A*, 526, A60. 1009.6065